Geometric and Hydrodynamic Characteristics of Three-dimensional Saturated Prefractal Porous Media Determined with Lattice Boltzmann Modeling

Jung-Woo Kim, Michael C. Sukop, Edmund Perfect, Yakov A. Pachepsky & Heechul Choi

Transport in Porous Media

ISSN 0169-3913

Transp Porous Med
DOI 10.1007/s11242-011-9818-6

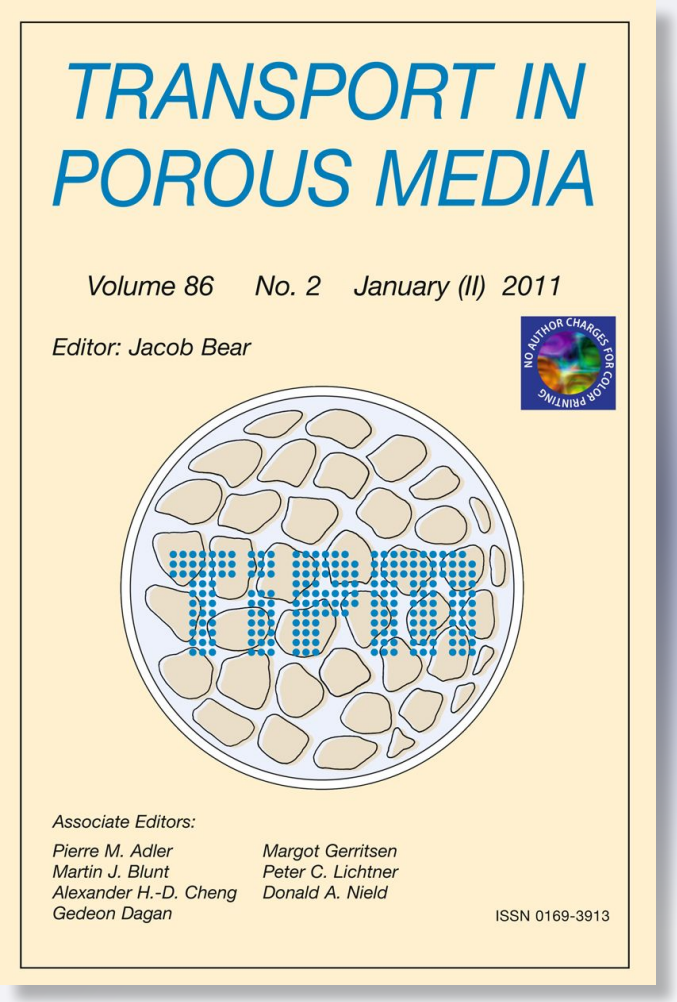

Springer

Transp Porous Med
DOI 10.1007/s11242-011-9818-6

Geometric and Hydrodynamic Characteristics of Three-dimensional Saturated Prefractal Porous Media Determined with Lattice Boltzmann Modeling

Jung-Woo Kim · Michael C. Sukop · Edmund Perfect · Yakov A. Pachepsky · Heechul Choi

Received: 27 April 2010 / Accepted: 29 July 2011

Abstract Fractal and prefractal geometric models have substantial potential for contributing to the analysis of flow and transport in porous media such as soils and reservoir rocks. In this study, geometric and hydrodynamic parameters of saturated 3D mass and pore–solid prefractal porous media were characterized using the lattice Boltzmann model (LBM). The percolation thresholds of the 3D prefractal porous media were inversely correlated with the fraction of micro-pore clusters and estimated as 0.36 and 0.30 for mass and pore–solid prefractal porous media, respectively. The intrinsic permeability and the dispersivity of the 3D pore–solid prefractals were larger than those of the 3D mass prefractals, presumably because of the occurrence of larger solid and pore cluster sizes in the former. The intrinsic permeability and dispersivity of both types of structure increased with increasing porosity, indicating a positive relationship between permeability and dispersivity, which is at odds with laboratory data and current theory. This discrepancy may be related to limitations of the convection dispersion equation at the relatively high porosity values employed in the present study.

Keywords 3D fractal porous medium · Lattice Boltzmann model · Percolation threshold · Permeability · Dispersivity

J.-W. Kim (✉)
Radioactive Waste Technology Development Division, Korea Atomic Energy Research Institute (KAERI), 1045 Daedeok-daero, Yuseong-gu, Daejeon 305-353, Republic of Korea
e-mail: jw_kim@kaeri.re.kr

J.-W. Kim · Y. A. Pachepsky
USDA-ARS, 10300 Baltimore Ave., Beltsville, MD 20705, USA

M. C. Sukop
Department of Earth and Environment, Florida International University, Miami, FL 33199, USA

E. Perfect
Department of Earth and Planetary Science, University of Tennessee, Knoxville, TN 37996-1410, USA

H. Choi
Department of Environmental Science and Engineering, Gwangju Institute of Science and Technology (GIST), 1 Oryong-dong, Buk-gu, Gwangju 500-712, Republic of Korea

Published online: 11 August 2011

1 Introduction

Geometric and hydrodynamic characterizations of porous media (Rashidi et al. 1996) and fracture networks (Berkowitz 2002) are challenging areas of research. Applying fractal models to such systems is attractive since information about complexity at different scales is captured in a small number of parameters (Mandelbrot 1982). Fractal (covering an infinite range of scales) and prefractal (covering a finite range of scales) geometric models have been applied by many researchers to soils (e.g., Rieu and Perrier 1998) and rocks (e.g., Garrison et al. 1992) and show substantial potential for contributing to an improved understanding of flow and transport in porous media (Adler and Thovert 1993; Yu 2008) and for revealing relationships between geometrical parameters and flow and transport in hierarchical and heterogeneous systems (e.g., Gimenez et al. 1997; Xu 2004; Xu and Dong 2004; Xu and Yu 2008; Cihan et al. 2009).

Prefractal porous media can be created by the repeated application of a generator pattern onto itself (Mandelbrot 1982). If the iterative phase is composed solely of solids (or pores), the result is a mass (or pore) prefractal. Pore–solid prefractals (PSF) are generated when the iterative phase is composed of both voids and solids (Perrier et al. 1999). Mass prefractals consist of different-sized pores and small uniformly-sized solid particles, while pore prefractals are made up of different-sized solid particles separated by small uniformly-sized pores. The Sierpinski carpet (Tarafdara et al. 2001) and Menger sponge (Cihan et al. 2009) would be good examples of 2D and 3D mass prefractals, respectively. PSF contain both solid- and pore-size distributions, and thus are expected to be the most physically heterogeneous. All three types of fractals have been used as models of natural porous media (Katz and Thompson 1985; Garrison et al. 1992; Perrier et al. 1999).

Pore structure controls hydrodynamic characteristics of porous media at the pore scale (Dullien 1991). In particular, flow and transport can only occur within connected pore clusters. The percolation threshold is the critical value of pore occupation probability (or porosity in porous media) under which percolation is unlikely to occur and over which percolation is likely to occur. The percolation threshold of a randomly distributed binary square matrix (2D Bernoullian or Euclidean lattice in which the distribution of pores and solids lacks any spatial correlation) was empirically determined to be $\sim$0.5927 by several researchers (e.g., Lee 2007; Feng et al. 2008). Sukop et al. (2002) estimated percolation thresholds for the pore phase of homogeneous random 2D prefractal porous media as a function of their fractal parameters. However, to our knowledge, no studies have yet been published on the percolation thresholds of 3D prefractal porous media.

Permeability is an important parameter in determining the hydrodynamic characteristics of porous media. The heterogeneous and disordered geometry of rocks and soil, however, makes it difficult to analytically estimate the permeability of such materials. Permeability is often related to porosity based on the Kozeny–Carman (KC) equation, a semi-empirical model that is widely used to predict flow through porous media. Permeability can also be estimated by modeling porous media as fractals (e.g., Xu and Dong 2004; Yu and Liu 2004). Succi et al. (1989) first introduced 3D lattice Boltzmann models (LBMs) in complex geometries to estimate the permeability based on Darcy's law. From numerical simulations using LBM in 3D porous geometries, Cancelliere et al. (1990) concluded that the calculated permeabilities compared well with the theoretical results, including Brinkman's effective-medium theory at high porosity ($>$0.8) and the KC equation at low porosity. Recently, Cihan et al. (2009) evaluated the intrinsic permeability of mass fractal (MF) porous media using two new analytical models based on probabilistic approaches and the LBM. In addition, the LBM

was numerically demonstrated for diffusion in 2D fractal media and Taylor hydrodynamic dispersion (Cali et al. 1992).

Since the basic elements of the theory of the LBM for fluid dynamics were reviewed by Benzi et al. (1992), Wolf-Gladrow (2000), and Succi (2001), the LBM has been shown to be comparable with, or superior to, the finite-difference method for solving the steady-state Stokes equation within complex pore space geometries (Humby et al. 2002; Manwart et al. 2002). As a result, the LBM has been efficiently and extensively applied to simulate flow and transport in disordered porous media (e.g., White et al. 2006; Lehmann et al. 2008). In this technique, the Boltzmann equation is discretized and the fluid flow under a pressure gradient is computed for the determination of intrinsic permeability. No coupled data on permeability and dispersivity of 3D prefractal porous media have been obtained to date.

The main objective of this study was to estimate key geometric and hydrodynamic parameters (using the LBM method) of saturated 3D prefractal porous media. The geometric parameters investigated were porosity, effective porosity, fractal dimension, normalized lacunarity, and the percolation threshold. The hydrodynamic parameters investigated were the intrinsic permeability and dispersivity.

2 Materials and Methods

2.1 3D Prefractal Porous Media

The 3D prefractal porous media were generated using the homogeneous algorithm (Sukop et al. 2002) which was previously implemented in 2D by Kim et al. (2007) in the study of anomalous diffusion in prefractal porous media. MF and PSF porous media were considered in the present study. To construct a 3D MF, a solid initiator cube is subdivided into smaller cubes whose sizes are $1/b^3$ where b is a scaling factor at the first iteration. A fixed number of the smaller solid cubes, N_{ex}, is removed to form pores. The same procedure of removing N_{ex} smaller cubes, whose sizes are $1/b^{3\times n}$ where n is the iteration number, is applied to each of the remaining solid cubes from the previous iteration step. The locations of the remaining solid cubes at each step can be either predetermined (deterministic MF) or random (randomized MF). The porous medium becomes prefractal for any finite iteration. The method of constructing a 3D PSF differs from that used for the 3D MF in selecting the solid cubes for further pore space creation. In the case of a MF, all of the remaining solid cubes are scaled down. For a 3D PSF, however, only a limited number of solid cubes, N_{gen}, are subject to removal of solid material, while the rest remain solid. Therefore, large solid cubes can exist in the PSF, but not in the MF structures.

In this study, randomized MF and PSF were constructed by varying only N_{ex} with constant $b = 3, n = 3$, and $N_{gen} = 10$. Theoretically, N_{ex} must be less than b^3 in MF and $b^3 - N_{gen}$ in PSF. Therefore, N_{ex} was varied from 1 to 26 in MF and from 1 to 16 in PSF. The resulting size of the 3D prefractal porous media became $3^3 \times 3^3 \times 3^3$ voxels contained within a cube of unit side length (Fig. 1). For the statistical analysis of the geometric and hydrodynamic characteristics of the 3D randomized MF and PSF structures, 100 realizations of each porous medium were constructed for each N_{ex} value. The geometric characteristics were estimated using all of the 100 random realizations, while the hydrodynamic characteristics were estimated using 10 realizations (chosen at random) due to the time requirements of the single-processor LBM computations.

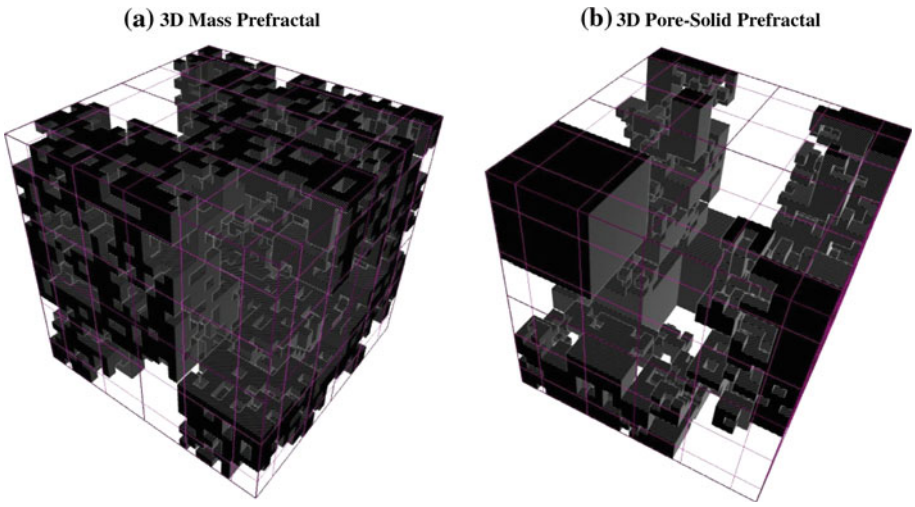

Fig. 1 Representative images of 3D MF (**a**) and PSF (**b**) porous media. ($b = 3, n = 3, N_{\text{gen}} = 10$, and $\phi = \sim 0.6$)

2.2 Geometric Characteristics

The porosity, ϕ, of the 3D prefractal porous media can be computed using the fractal parameters, b, n, N_{ex}, and N_{gen} (Kim et al. 2007):

$$\begin{cases} \phi = 1 - \left(1 - \frac{N_{\text{ex}}}{b^3}\right)^n & \text{for MF} \\ \phi = \frac{N_{\text{ex}}}{b^3 - N_{\text{gen}}} \left(1 - \left(\frac{N_{\text{gen}}}{b^3}\right)^n\right) & \text{for PSF} \end{cases} . \tag{1}$$

Since N_{ex} was the only variable used in the construction of the 3D MF and PSF structures in this study, ϕ is only a function of N_{ex} in Eq. 1.

Fractal dimension, D_{f}, is the most commonly used parameter in the characterization of prefractal porous media because it provides an objective means of relating the fractal geometric model to real porous media (Huang and Zhang 2005). The fractal dimensions of the 3D MF and PSF structures can be computed from their construction parameters; see Sukop et al. (2002) for MF and Perrier et al. (1999) for PSF:

$$\begin{cases} D_{\text{f}} = \frac{\log(b^3 - N_{\text{ex}})}{\log b} & \text{for MF} \\ D_{\text{f}} = \frac{\log N_{\text{gen}}}{\log b} & \text{for PSF} \end{cases} . \tag{2}$$

Since ϕ and D_{f} were computed using Eqs. 1 and 2, they were constant for all of the 100 realizations of each randomized prefractal porous medium.

Lacunarity, L, provides a quantitative measure of the spatial distribution of pores within a porous medium (Pendelton et al. 2005). If $\phi = 0$, L goes to infinity, and if $\phi = 1$, L becomes one. At a given ϕ, larger L values imply many large pores and/or coalescence of smaller pores into larger ones, whereas smaller L values imply many scattered small pores with little or no pore clustering. Lacunarity was calculated using the gliding box method suggested by Allain and Cloitre (1991):

$$L(r) = \frac{\sum_p p^2 Q(p,r)}{\left(\sum_p pQ(p,r)\right)^2}, \tag{3}$$

where p is the number of pore voxels in a gliding cube of size r^3 in the 3D porous media, and $Q(p,r)$ is the pore probability distribution function. The scale dependency of $L(r)$ in Eq. 3 can be estimated by varying the gliding window size, r, with L known to be inversely proportional to r for MF (Turcotte 1997). Plotnick et al. (1996) defined the maximum L, $L_{\max}$, as $1/\phi$ when $r = 1$ and the minimum L, $L_{\min}$, as unity when $r = b^n$.

Since L is intended as a measure of pore clustering, the meaning of L can be blurred if ϕ changes. Therefore, so that porous media with different porosities could be compared, we normalized L following Roy et al. (2010) normalization approach:

$$L^*(r) = \frac{L(r) - L_{\min}}{L_{\max} - L_{\min}} = \frac{L(r) - 1}{1/\phi - 1}, \tag{4}$$

where $L_{\min}$ and $L_{\max}$ are the theoretical minimum and maximum values of lacunarity, respectively, and L^* is the normalized lacunarity. The gliding window size, r, is generally a multiple of the scaling factor b. In this study, r was taken equal to 3, 9, 15, and 21.

A pore cluster in a porous medium was defined as a set of pores connected side-by-side. Pore clusters were identified using the Hoshen–Kopelman algorithm (Hoshen and Kopelman 1976). The size (volume) of a pore cluster was quantified by counting pore voxels. In this study, the "infinite pore cluster" was defined as the pore cluster which connected one side of the porous medium to the other side. Flow and transport will not occur at all in absence of the infinite pore cluster. The percolation threshold is the critical value of porosity above which the porous medium's pores percolate and below which they do not. Since the percolation threshold is not as sharply defined in finite systems, the percolation threshold was determined as the porosity where the percolation frequency is 50% (Sukop et al. 2002). Accordingly, the percolation frequency was estimated from 100 random realizations for each condition. For a percolating porous medium, the percolating pore cluster was characterized by its porosity, which is termed the effective porosity, ϕ_{eff} ($0 \le \phi_{\text{eff}} \le \phi$). If a porous medium does not percolate, its ϕ_{eff} will be zero. A large difference between ϕ and ϕ_{eff} may imply that the percolating pore cluster is rather narrow and/or directly connected by small pores. Otherwise, the percolating pore cluster is rather wide and/or comprised of large pores. Since flow and transport can occur only in percolating porous media, hydrodynamic characteristics were only computed for those structures where the porosity was larger than the percolation threshold for each prefractal porous medium.

2.3 Lattice Boltzmann Model (LBM)

A LBM was applied to compute the hydrodynamic characteristics of the saturated 3D prefractal porous media. Detailed introductions to the LBM for 2D porous media can be found in Sukop and Thorne (2006) and Wolf-Gladrow (2000). The following brief description of the 3D LBM is principally based on Sukop and Thorne (2006) work in 2D. The 3D LBM was implemented in terms of both fluid and solute components to simulate flow and transport.

The evolution of the fluid density distribution function, f, is based on the following lattice Boltzmann equation:

$$f_a(\mathbf{x} + \mathbf{e}_a \Delta t, t + \Delta t) = f_a(\mathbf{x}, t) - \frac{\left[f_a(\mathbf{x}, t) - f_a^{\text{eq}}(\mathbf{x}, t)\right] \cdot \Delta t}{\tau}, \tag{5}$$

where $f_a(\cdot)$ is the fluid density distribution function in the ath velocity direction, $\mathbf{x}$ is the position vector (x, y, z), t and Δt are the time and the time increment, respectively, τ is the single relaxation time which controls the rate of approach to equilibrium, and the unit velocity vector, $\mathbf{e}_a$, in the D3Q19 model (3 dimensions and 19 directions of unit velocity), which was applied into this study, is defined as:

$$\begin{pmatrix} \mathbf{e}_{a(x)} \\ \mathbf{e}_{a(y)} \\ \mathbf{e}_{a(z)} \end{pmatrix} = \begin{bmatrix} 0 & \pm 1 & 0 & 0 & \pm 1 & \pm 1 & 0 \\ 0 & 0 & \pm 1 & 0 & \pm 1 & 0 & \pm 1 \\ 0 & 0 & 0 & \pm 1 & 0 & \pm 1 & \pm 1 \end{bmatrix}. \tag{6}$$

The equilibrium distribution function in the ath velocity direction, f_a^{eq}, takes the form of a quadratic expansion of the Maxwellian (Qian et al. 1992):

$$f_a^{\mathrm{eq}} = w_a \rho \left(1 + \frac{1}{3}\, \mathbf{e}_a \cdot \mathbf{u} + \frac{9}{2}\, (\mathbf{e}_a \cdot \mathbf{u})^2 - \frac{3}{2}\, \mathbf{u} \cdot \mathbf{u} \right), \tag{7}$$

where ρ is the fluid density, $\mathbf{u} = (u_x, u_y, u_z)$ is the fluid velocity vector, and w_a is the direction-specific weight: $w_a = 1/3$ $(a = 1)$, $w_a = 1/18$ $(a = 2, \ldots, 7)$, and $w_a = 1/36$ $(a = 8, \ldots, 19)$. The macroscopic properties of fluid density and velocity were computed by incorporating $f_a(\cdot)$ and $\mathbf{e}_a$ based on mass and momentum conservation:

$$\rho = \sum_{a=1}^{19} f_a \text{ and} \tag{8}$$

$$\mathbf{u} = \frac{1}{\rho} \sum_{a=1}^{19} f_a \mathbf{e}_a. \tag{9}$$

The fluid kinematic viscosity, ν, in the LBM is defined as:

$$\nu = \frac{1}{3} \left(\tau - \frac{1}{2} \right). \tag{10}$$

The LBM uses modeling units such as lattice unit (lu) for length, time unit (ts) for time, and mass unit (mu) for mass. The value of τ was set to unity leading to $\nu = 1/6\,\mathrm{lu}^2\,\mathrm{ts}^{-1}$ in order to eliminate any ambiguity on the effective location of the solid boundary.

The solute density distribution function, f_c, can also be defined based on Eq. 5 by replacing f_a with $f_{c,a}$. The equilibrium distribution function for the solute component, $f_{c,a}^{\mathrm{eq}}$, is:

$$f_{c,a}^{\mathrm{eq}} = w_a C \rho \, (1 + 3\, \mathbf{e}_a \cdot \mathbf{u}), \tag{11}$$

where C is the solute concentration, which is defined by the following equation:

$$C = \frac{\sum_{a=1}^{19} f_{c,a}}{\rho}. \tag{12}$$

The definition of the kinematic viscosity (ν in Eq. 10) for the fluid component can also be used to determine the molecular diffusion coefficient ($D_w = 1/6\,\mathrm{lu}^2\,\mathrm{ts}^{-1}$) for the solute component.

Fluid flow was induced in the z-direction. The boundary conditions of the fluid flow at the inlet and outlet were constant flux ($0.001\,\mathrm{lu\,ts}^{-1}$) and constant pressure ($1.000\,\mathrm{mu\,lu}^{-3}$) conditions, respectively. The fluid was forced to flow from the boundary conditions. The pressure at the inlet due to the hydrodynamic resistance of the porous medium was computed.

The unknown directional flow densities, f_{a_1}, at the boundary nodes were computed using the macroscopic density and velocity formulas (Eqs. 8 and 9). For the solute component, constant and no-gradient concentration boundary conditions were applied to the inlet and outlet, respectively. Following Sukop and Thorne (2006) work in the 2D domain, the unknown directional solute densities, f_{c,a_1}, in D3Q19 were determined as:

$$f_{c,a_1} = w_{a_1} \cdot \frac{C\rho - \sum_{a_2} f_{c,a_2}}{w_2 + 4 \cdot w_8}, \tag{13}$$

where a_1 and a_2 indicate unknown and known directions, respectively, at the boundary; a_1 could be (7, 14, 15, 18, 19) at the inlet and (6, 12, 13, 16, 17) at the outlet. All other side boundaries were treated with a periodic boundary condition.

When the LBM was used for hydrodynamic characterization, buffer spaces (2-layers of pore space for each inlet and outlet: dimensions $= 3^3 \times 3^3 \times (3^3 + 2 + 2)\,\mathrm{lu}^3$) were located at the inlets and outlets of the prefractal porous media to prevent a sudden hydrodynamic change at these boundaries.

2.4 Hydrodynamic Characteristics

Each prefractal porous medium was characterized by its intrinsic permeability and dispersivity. The intrinsic permeability, k, was computed by invoking Darcy's law:

$$k = \frac{q\overline{\rho}\nu}{d\psi/l_z}, \tag{14}$$

where q is the Darcy flux which equals $\overline{u}_z \cdot \phi$ ($\overline{u}_z$ is the averaged pore velocity in z-direction over the porous medium), $\overline{\rho}$ is the average of the fluid densities over the porous medium, l_z is the length of the porous medium in the z-direction, and $d\psi$ is the pressure difference between the inlet and outlet. The pressure was calculated from the Equation of State, $\psi = \rho/3$ (Sukop and Thorne 2006). The k was computed at each time step until it became constant. The average Reynolds numbers (Re) were in the range from 0.22 to 0.37 and suggested that the k was estimated under creeping flow conditions (i.e., $Re < 1$).

The dispersivity, λ, was computed using its relationship with the dimensionless Peclet number ($Pe = \overline{u}_z \cdot l_z/D = l_z/\lambda$) where D is the dispersion coefficient. The value of Pe was estimated from nonlinear regression of the analytical solution of the convection-dispersion equation (CDE) with constant concentration at inlet and no-gradient concentration at outlet for finite systems (Cleary and Adrian 1973):

$$\frac{C}{C_0} = 1 - \sum_{m=1}^{\infty} \frac{2\beta_m \sin(\beta_m) \exp\left[\frac{Pe}{2} - \frac{Pe \cdot T}{4R_t} - \frac{\beta_m^2 T}{Pe \cdot R_t}\right]}{\beta_m^2 + \frac{Pe^2}{4} + \frac{Pe}{2}}. \tag{15}$$

Here, T is dimensionless time (pore volume $= t \cdot \overline{u}_z/l_z$), R_t is the retardation factor ($= 1$ for a nonreactive solute), and the eigenvalues, β_m, are the positive roots of the equation:

$$\beta_m \cot(\beta_m) + \frac{Pe}{2} = 0 \tag{16}$$

3 Results and Discussion

3.1 Geometric Characteristics of Prefractal Porous Media

The porosity, ϕ, of the 3D MF and PSF structures generated in this study ranged from 0.107 to 1.000 and from 0.056 to 0.893, respectively (Fig. 2). It increased logarithmically for MF and linearly for PSF as N_{ex} increased. In contrast to the 3D MF structures, at least one solid voxel remains at each iteration level for the 3D PSF structures because of the difference between the values of $b^3 - N_{ex}$ and N_{gen}. Therefore, the maximum ϕ for the PSF porous media was generally less than that for the MF porous media and the minimum ϕ of the PSF porous media was generally larger than that for the MF porous media (Fig. 2). The maximum ϕ of the 3D PSF structures will be closer to unity as the value of b is increased. The fractal dimension, D_f, of 3D MF structures was inversely proportional to ϕ. In contrast, the D_f of a 3D PSF is independent of N_{ex} in Eq. 2, but depends only on N_{gen}, which was a constant in this study. Therefore, the D_f of the 3D PSF structures was 2.096 (=log 10/log 3) regardless of the value of ϕ (Fig. 2).

Figure 3 shows contour maps of the normalized lacunarity, L^*, distributions in the two different structure types with varying ϕ and gliding window size. As expected, the dependence of lacunarity on porosity was substantially removed by the normalization. The L^* decreased as the gliding window size increased in both types of porous media. The L^* of the 3D PSF structures was more sensitive to the gliding window size as compared to that for the 3D MF structures, and larger values of L^* were observed for the 3D PSF structures as compared to the 3D MF structures at any given ϕ and gliding window size. The main difference between the 3D MF and PSF structures is that only the 3D PSF structures have large solid cubes which may cause larger pore clusters at certain ϕ values (e.g., Fig. 1). Kim et al. (2007) pointed out that the presence of large solid squares in 2D PSF porous media induced greater pore cluster clumping compared to 2D MF porous media.

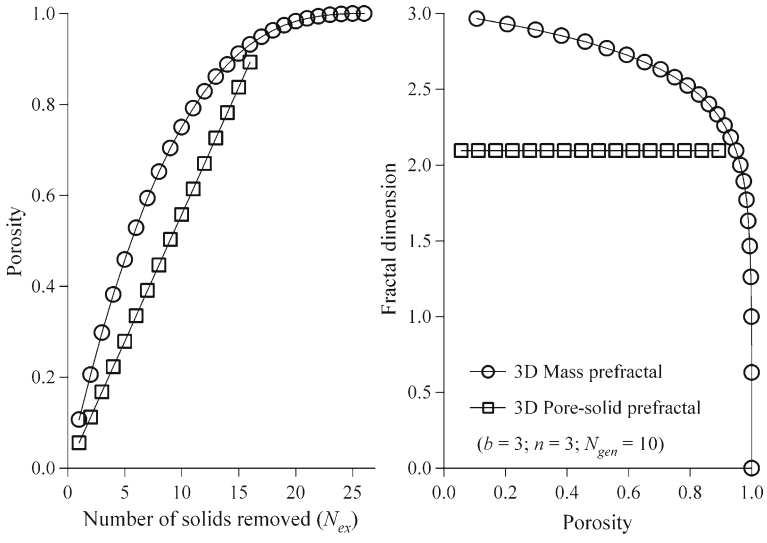

Fig. 2 Variations of porosities and fractal dimensions of 3D MF and PSF porous media generated in this study. ($b = 3$, $n = 3$, $N_{gen} = 10$, and $\phi = \sim 0.6$)

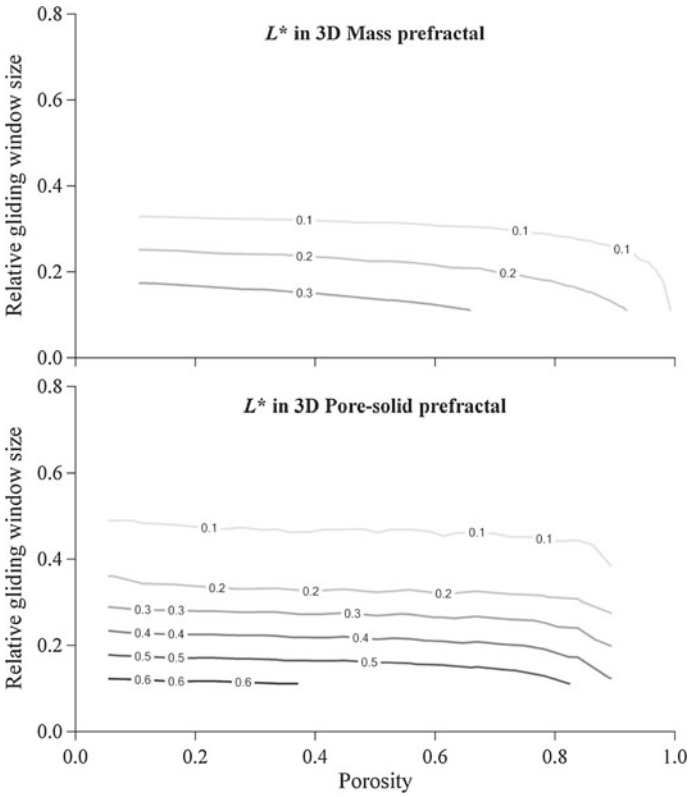

Fig. 3 Contour maps of normalized lacunarity (L^*) distributions in 3D MF and PSF porous media varying porosity and gliding window size

Based on the 100 random realizations, the average pore cluster size distributions of the 3D MF and PSF structures for different ϕ values are plotted in Fig. 4 along with their 95% confidence intervals in order to see how the pores are distributed in the porous media. Pore cluster sizes were classified into 10 groups in terms of the ratio to the total volume of the porous medium (e.g., pore cluster size 0.0–0.1 means the volume of pores whose size are between 0.0 and 0.1 when the total volume of porous medium equals 1). In both MF and PSF structures, the pore space was dominated by a single large pore cluster at high ϕ and by many small pore clusters at low ϕ. The proportion of small pore clusters in the pore space decreased with increasing ϕ. The existence of large pore voxels in the 3D PSF structures induced larger pore clusters than in the 3D MF structures at the same ϕ ranging from $\sim$0.2 to $\sim$0.7. The results implied that the porous media with low porosity would consist of many scattered and isolated small pore clusters while the porous media with high porosity would consist of a few large pore clusters.

The percolation frequencies of the 3D MF and PSF structures as a function of ϕ are shown in Fig. 5. All MF and PSF structures percolated when ϕ was larger than 0.45. As ϕ decreased below 0.45, the percolation frequency decreased and the porous media never percolated when ϕ was below 0.206 and 0.112 for the MF and PSF structures, respectively. From linear interpolation with data of Fig. 5, the porosity thresholds for percolation in the 3D MF and PSF structures (defined as the 50% percolation frequency) were estimated as

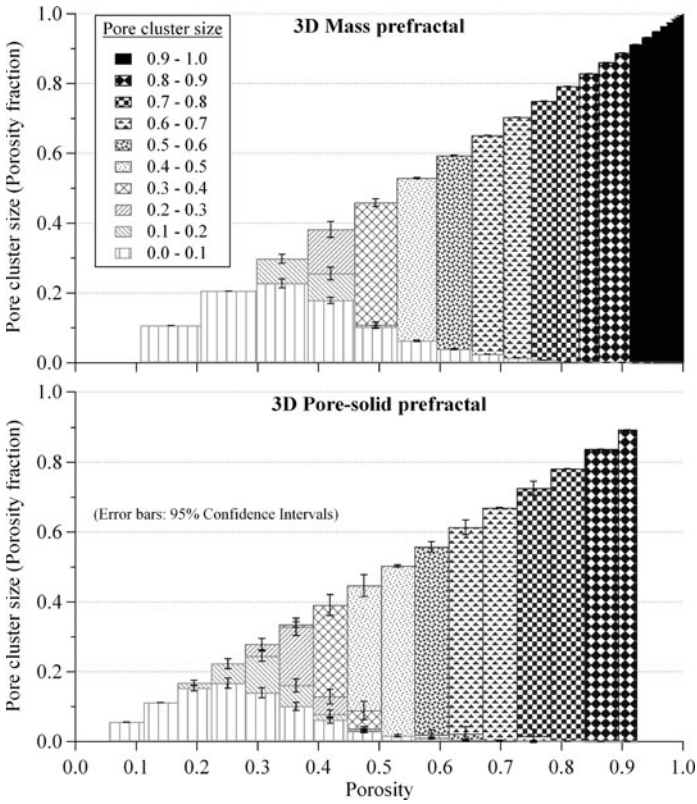

Fig. 4 Pore cluster size distributions of 3D MF and PSF porous media for 100 realizations

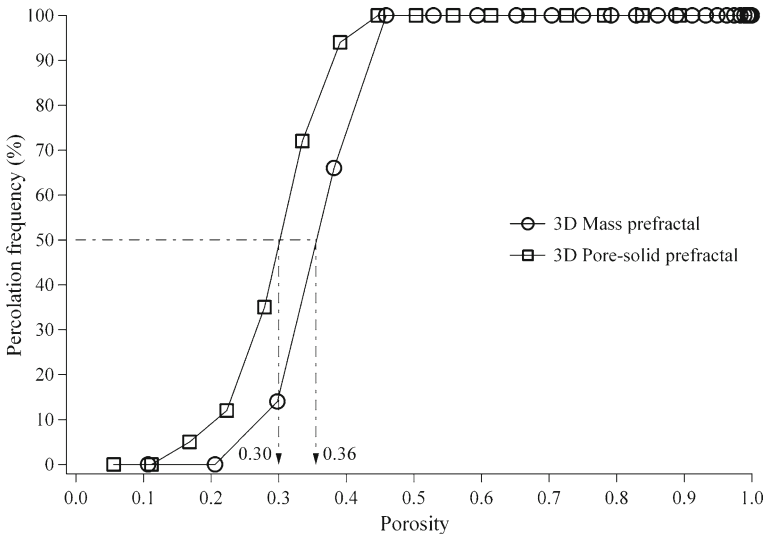

Fig. 5 Percolation frequencies of 3D MF and PSF depending on porosity for 100 realizations

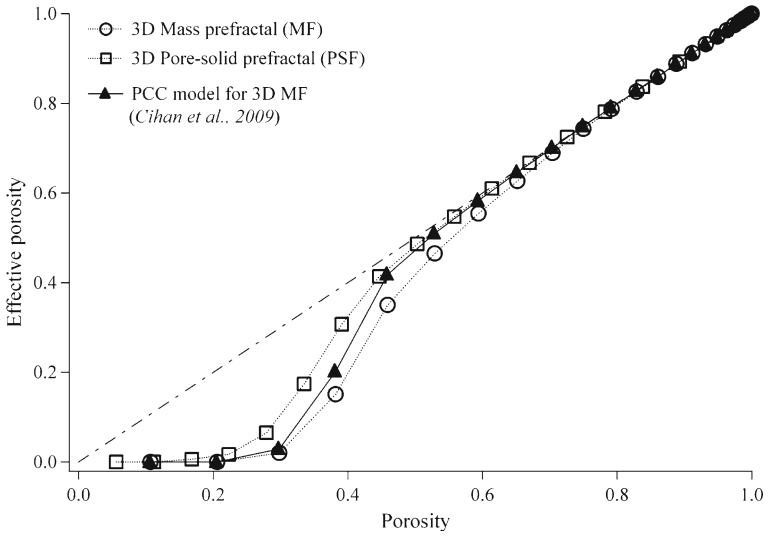

Fig. 6 Averages of the effective porosity of 3D mass and pore–solid prefractals for 100 realizations and Cihan et al. (2009) analytical estimation of effective porosity of 3D MF depending on porosity. (95% confidence intervals were mostly smaller than the symbols, with maximum value of 0.029 when porosity is 0.38)

∼0.36 and ∼0.30, respectively. As expected from the behavior of Bernoullian or Euclidean structures, the percolation threshold of the 3D MF porous media estimated in this study (∼0.36) was much smaller than that of the 2D MF porous media determined by Sukop et al. (2002) (0.708 ± 0.060 when $b = 3$ and $n = 3$). Our estimate for the 3D PSF structures (∼0.30) was very close to the value for site percolation threshold in Bernoullian or Euclidean 3D binary porous media which is 0.3116 (Stauffer and Aharony 1994).

The proportions of micro-pore clusters sized between 0.0 and 0.1 appeared to be inversely correlated with the percolation frequency. The fraction of micro pores was ∼50% when $\phi = 0.38$ in the 3D MF structures and 0.28 in the 3D PSF structures. Interestingly, these ϕ values were similar to the percolation thresholds for each porous medium. That is, the fractions of micro pores were larger than 50% when ϕ was less than the percolation threshold. These results imply that knowledge of the fraction of micro pores and/or pore cluster size distribution (as in Fig. 4) for a porous medium can be an indicator to determine whether or not it percolates.

The average values of the effective porosity, ϕ_{eff}, are shown in Fig. 6. The 95% confidence intervals bounding the average values were relatively small having a maximum value of 0.029 when the porosity was 0.38. Connectivity of 3D PSF structures, which had more large solid cubes and thus larger pore clusters at the same ϕ, was greater when compared to the 3D MF structures, especially when ϕ was in the percolation transition zone (i.e., between $\phi = 0.2$ and 0.5). When ϕ was larger than 0.7, the ϕ_{eff} of both the 3D MF and PSF structures were almost equal to ϕ. The ϕ_{eff} of the 3D MF structures was also computed by the probabilistic capillary connectivity (PCC) model of Cihan et al. (2009) using the fractal parameters b, n, and D_{f}:

$$\phi_{\text{eff}} = \sum_{i=1}^{n} \sum_{j=i}^{n} \frac{\left(b^3 - b^{D_{\text{f}}}\right) \cdot b^{(i-1)D_{\text{f}}}}{b^{3i}} \cdot P \cdot (1-P)^{(j-i)}, \tag{17}$$

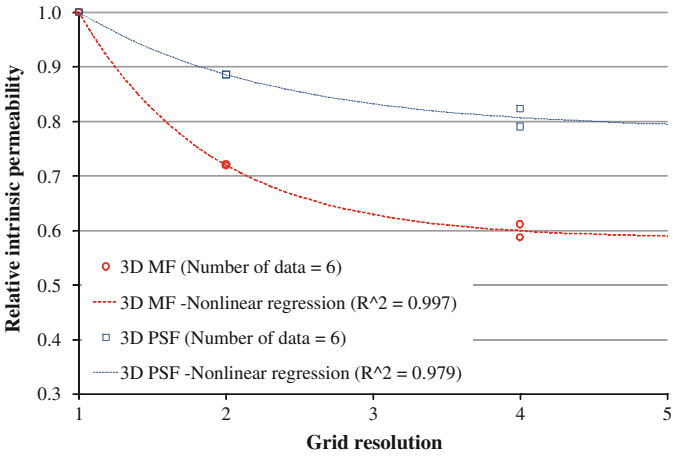

Fig. 7 Dependencies of LBM intrinsic permeabilities on the grid resolution for **a** 3D MF ($\alpha = 0.585$ and $\beta = 1.124$ in Eq. 18) and **b** PSF ($\alpha = 0.784$ and $\beta = 0.754$ in Eq. 18)

where P is the fraction of connected pores. At low ϕ ($\phi < 0.3$) and high ϕ ($\phi > 0.7$), the ϕ_{eff} predictions of the PCC model closely matched those computed from the Hoshen–Kopelman algorithm used in this study. When ϕ was between 0.3 and 0.7, the PCC model slightly overestimated values for the 3D MF.

3.2 Hydrodynamic Characteristics of Prefractal Porous Media

Hydrodynamic characteristics were computed for $\phi = 0.53, 0.59$, and 0.70 and $\phi = 0.50, 0.61$, and 0.73 of the 3D MF and PSF structures, respectively. As ϕ increased, the average intrinsic permeability, k, computed by the LBM increased from 0.045 to 0.573 lu^2 in the 3D MF structures and from 0.129 to 1.704 lu^2 in the 3D PSF structures. Pan et al. (2006) suggested that estimates of k may depend upon the resolution of the porous medium. To account for this effect, the values of k were corrected for grid resolution using the following nonlinear regression equation:

$$\frac{k_{Rs}}{k_1} = (1 - \alpha) \cdot \exp\left(-\beta \cdot (Rs - 1)\right) + \alpha, \tag{18}$$

where Rs is the grid resolution, and α and β are the regression parameters. From curve-fitting conducted using k data for the lowest and highest porosities for each structure with $Rs = 1$, 2, and 4 (i.e., 6 data points per fit), α and β were estimated as 0.585 and 1.124 for MF and 0.784 and 0.754 for PSF, respectively. The two regression equations were independent of the porosity but dependent upon the type of porous medium (Fig. 7). Based on these results, the raw k values were modified as the asymptotic values of Eq. 18 assuming $Rs \rightarrow$ infinity.

One way analysis of variance (ANOVA) with replication combined with student's t-tests (i.e., protected t-tests) indicated significant differences (at $P < 0.05$) in the mean values of the resulting resolution-corrected intrinsic permeabilities among the three different porosity classes investigated (Table 1). The mean k values increased with increasing porosity and were generally higher for the 3D PSF porous media as compared to the 3D MF porous media. The differences in intrinsic permeability between the two prefractal models increased with increasing ϕ.

Table 1 Mean intrinsic permeability (k) and dispersivity values (λ) obtained for 3D mass (MF) and pore–solid (PSF) prefractals with different porosities using LBM

MF					PSF		
ϕ	k	k_{PCC}	k_{MPA}	λ	ϕ	k	λ
0.53	$0.07^{A\dagger}$	0.21^{A}	0.18^{A}	44.3^{A}	0.50	0.20^{A}	57.4^{A}
0.59	0.11^{B}	0.34^{B}	0.24^{B}	58.7^{B}	0.61	0.55^{B}	86.2^{B}
0.70	0.26^{C}	0.58^{C}	0.38^{C}	90.4^{C}	0.73	1.02^{C}	103.3^{C}

Cihan et al. (2009) PCC and MPA analytical estimates of intrinsic permeability for 3D MF structures are also included

† Mean values within a column with the same superscript letter are not significantly different at $P < 0.05$

The resolution-corrected k values of the 3D MF structures estimated by LBM simulation in this study were compared with the k values computed by Cihan et al. (2009) two analytical expressions; i.e., the PCC model:

$$k = C_p b^{2n} \sum_{i=1}^{n} \sum_{j=i}^{n} \frac{\left(b^3 - b^{D_f}\right) \cdot b^{(i-1)D_f}}{b^{3i+2j}} \cdot P \cdot (1-P)^{(j-i)}, \tag{19}$$

and Marshall's probabilistic approach (MPA) model:

$$k = C_p b^{2n} \frac{\left(b^2 - b^{(D_f-1)}\right)^2 \left(b^4 + b^{(D_f-1)}\right)}{\left(b^4 - b^{(D_f-1)}\right)\left(b^6 - b^{2(D_f-1)}\right)}, \tag{20}$$

where C_p is a pore shape factor (=0.035 for square). The estimates of k from both the PCC and MPA models were slightly larger than the k values obtained using the LBM, but exhibited similar functional dependencies upon the porosity (Table 1). Cihan et al. (2009) concluded that the PCC model might be more reliable for computing permeability in heterogeneous fractal porous media because the PCC model considers the measure of connectivity due to randomizations while the MPA model can capture only the average permeability. However, in our study the MPA model predictions were most consistent with the independent LBM results.

The modeling unit, lu^2, of k can be converted to physical units using the scale conversion factor as follows:

$$k_{physical} = k_{LBM} \cdot \left(\frac{l_{physical}}{l_{LBM}}\right)^2, \tag{21}$$

where $l_{physical}$ is the physical length comparable with the modeling length unit in LBM, l_{LBM}. If one lu (the length unit of LBM) equals 10 μm in physical length units, the total volume of the porous media employed in this study is $(27 \times 10)^3 \mu m^3$, with the average k of the 3D MF and PSF structures ranging from 2.63 μm^2 to 33.52 μm^2 and from 10.11 to 133.59 μm^2, respectively.

The average dispersivity values for the 3D PSF structures were generally higher than those for the 3D MF structures, and both of the estimates approached ~100 lu at $\phi \geq 0.7$ (Table 1). Generally, dispersion is expected to be proportional to the average solid size of the porous medium (Bear 1988). Since only the 3D PSF structures had a particle size distribution (Fig. 1), their higher λ values may be attributable to the presence of large solid particles within the flow domain. For $\phi \geq 0.7$, however, the impact of these large particles is reduced, resulting in similar λ values.

Dispersivity increased with increasing ϕ for both the 3D MF and PSF porous media (Table 1). In previous studies, a negative relationship between ϕ and λ has been observed and seems physically reasonable, since the irregularity of flow paths within a porous medium should decrease with increasing ϕ, resulting in a decrease in λ. For instance, Xu and Eckstein (1997) and Perfect et al. (2002) showed that for experimental results with saturated soils and rocks there was a negative correlation between ϕ and λ for $\phi < 0.5$. However, the relationships between λ and ϕ for the saturated percolating 3D MF and PSF structures employed in this study were positive for $\phi > 0.5$. The following argument is proposed to explain this apparent discrepancy. It is possible that as the porosity increases, transport begins to deviate from that predicted by the convective–dispersive equation. Examination of the individual breakthrough curves (data not shown) revealed that the CDE sometimes over predicted the early part of the curve and under predicted the later part. Thus, the increase in dispersivity with porosity that we observed may be a consequence of the assumption of the applicability of the CDE at high porosity rather than the consequence of any actual physical mechanism. In this regard, further research is needed to investigate the applicability of other transport models, such as the mobile–immobile model (MIM) and the fractional advection dispersion equation (FADE) for describing transport in high porosity materials.

The positive relationships observed between k and ϕ and between λ and ϕ in Table 1 imply a positive relationship (confirmed by correction analysis; $r = 0.84$, $P < 0.05$) between λ and k. Again, such a relationship is physically hard to explain, and may be related to the proposed inapplicability of the CDE at high porosities. The theoretical approach used by Bear (1988) to relate dispersivity to the intrinsic permeability predicts an inverse relationship, as well as a functional dependence upon ϕ. In our case, k made no significant contribution to the prediction of λ once ϕ was included in a multiple regression model (results not shown). It is worth noting that the experimental data presented in Fig. 8 of Xu and Eckstein (1997) appear to exhibit two different responses: an inverse relationship between λ and k at low k values (low porosities) and a positive relationship at high k values (high porosities). Clearly, additional research is warranted on this issue.

4 Conclusions

Selected 3D mass, MF, and pore–solid, PSF, prefractal porous media were characterized in terms of their geometric parameters (porosity, effective porosity, fractal dimension, lacunarity, and percolation threshold), and hydrodynamic parameters (intrinsic permeability and dispersivity) determined using a Lattice Boltzmann model. Differences in the pore and solid size distributions of the 3D MF and PSF structures resulted in distinctly different characteristics for each porous medium model. In particular, the percolation thresholds of the 3D prefractal porous media were inversely correlated with the fraction of micro-pore clusters and estimated as 0.36 and 0.30 for MF and PSF structures, respectively. At porosities in the range from 0.5 to 0.7, prefractal porous media always percolated, and the intrinsic permeability and dispersivity of the 3D PSF structures were estimated to be higher than those of the 3D MF structures, presumably because of the larger solid and pore cluster sizes in the former. In the hydrodynamic characterization of 3D prefractal porous media, a LBM was used for fluid flow and for solute transport. Both the intrinsic permeability and dispersivity increased as the porosity of these structures increased. The underlying origins of these relations are not well understood, but may be related to limitations of the convection dispersion equation at high porosities.

References

Adler, P.M., Thovert, J.F.: Fractal porous-media. Transp. Porous Media **13**(1), 41–78 (1993)

Allain, C., Cloitre, M.: Characterizing the lacunarity of random and deterministic fractal sets. Phys. Rev. A **44**, 3552–3558 (1991)

Bear, J.: Dynamics of Fluids in Porous Media. pp. 106–118. Dover Publications, New York (1988)

Benzi, R., Succi, S., Vergassola, M.: The lattice Boltzmann equation: theory and applications. Phys. Rep. **222**(3), 145–197 (1992)

Berkowitz, B.: Characterizing flow and transport in fractured geological media: a review. Adv. Water Resour. **25**, 861–884 (2002)

Cali, A., Succi, S., Cancelliere, A., Benzi, R., Gramignani, M.: Diffusion and hydrodynamic dispersion with the lattice Boltzmann method. Phys. Rev. A **45**(8), 5771–5774 (1992)

Cancelliere, A., Chang, C., Foti, E., Rothman, D.H., Succi, S.: The permeability of a random medium: comparison of simulation with theory. Phys. Fluids A **2**(12), 2085–2088 (1990)

Cihan, A., Sukop, M.C., Tyner, J.S., Perfect, E., Huang, H.: Analytical predictions and lattice Boltzmann simulations of intrinsic permeability for mass fractal porous media. Vadose Zone J. **8**(1), 187–196 (2009)

Cleary, R.W., Adrian, D.D.: Analytical solution of convective-dispersive equation for cation adsorption in soils. Soil Sci. Soc. Am. J. **37**(2), 197–199 (1973)

Dullien, F.A.L.: Characterization of porous media—pore level. Transp. Porous Media **6**, 581–606 (1991)

Feng, X., Deng, Y., Blote, H.W.J.: Percolation transitions in two dimensions. Phys. Rev. E **78**, 031136 (2008)

Garrison, J.R., Pearn, W.C., Von Rosenberg, D.U.: The fractal Menger sponge and Sierpinski carpet as models for reservoir rock pore systems: 1, Theory and image-analysis of Sierpinski carpets. In Situ **16**(4), 351–406 (1992)

Gimenez, D., Perfect, E., Rawls, W.J., Pachepsky, Y.A.: Fractal models for predicting soil hydraulic properties: a review. Eng. Geol. **48**, 161–183 (1997)

Hoshen, J., Kopelman, R.: Percolation and cluster distribution. I. Cluster multiple labeling technique and critical concentration algorithm. Phys. Rev. B **14**, 3438–3445 (1976)

Huang, G., Zhang, R.: Evaluation of soil water retention curve with the pore–solid fractal model. Geoderma **127**, 52–61 (2005)

Humby, S.J., Biggs, M.J., Tuzun, U.: Explicit numerical simulation of fluids in reconstructed porous media. Chem. Eng. Sci. **57**, 1955–1968 (2002)

Katz, A.J., Thompson, A.H.: Fractal sandstone pores: implications for conductivity and pore formation. Phys. Rev. Lett. **54**, 1325–1328 (1985)

Kim, J.-W., Perfect, E., Choi, H.: Anomalous diffusion in two-dimensional Euclidean and prefractal geometric models of heterogeneous porous media. Water Resour. Res. **43**(1), W01405 (2007)

Lee, M.J.: Complementary algorithms for graphs and percolation. Phys. Rev. E **76**(2), 027702 (2007)

Lehmann, P., Berchtold, M., Ahrenholz, B., Tolke, J., Kaestner, A., Krafczyk, M., Fluhler, H., Kunsch, H.R.: Impact of geometric properties on permeability and fluid phase distribution in porous media. Adv. Water Resour. **31**, 1188–1204 (2008)

Mandelbrot, B.B.: The Fractal Geometry of Nature, pp. 1–24, 131–144. Freeman, New York, NY (1982)

Manwart, C., Aaltosalmi, U., Koponen, A., Hilfer, R., Timonen, J.: Lattice-Boltzmann and finite-difference simulations for the permeability for three-dimensional porous media. Phys. Rev. E **66**, 016702 (2002)

Pan, C., Luo, L.-S., Miller, C.T.: An evaluation of lattice Boltzmann schemes for porous medium flow simulation. Comput. Fluids **35**, 898–909 (2006)

Pendelton, D.E., Dathe, A., Baveye, P.: Influence of image resolution and evaluation algorithm on estimates of the lacunarity of porous media. Phys. Rev. E **72**(4), 041306 (2005)

Perfect, E., Sukop, M.C., Haszler, G.R.: Prediction of dispersivity for undisturbed soil columns from water retention parameters. Soil Sci. Soc. Am. J. **66**, 696–701 (2002)

Perrier, E., Bird, N., Rieu, M.: Generalizing the fractal model of soil structure: the pore–solid fractal approach. Geoderma **88**, 137–164 (1999)

Plotnick, R.E., Gardner, R.H., Hargrove, W.W., Prestegaard, K., Perlmutter, M.: Lacunarity analysis: a general technique for the analysis of spatial patterns. Phys. Rev. E **53**(5), 5461–5468 (1996)

Qian, Y.H., d'Humieres, D., Lallemand, P.: Lattice BGK models for Navier-Stokes equation. Europhys. Lett. **17**(6), 479–484 (1992)

Rashidi, M., Peurrung, L., Tompson, A.F.B., Kulp, T.J.: Experimental analysis of pore-scale flow and transport in porous media. Adv. Water Resour. **19**(3), 163–180 (1996)

Rieu, M., Perrier, E.: Fractal models of fragmented and aggregated soils. In: Baveye, P. (ed.) Fractals in Soil Science, Advances in Soil Science Series, pp. 169–202. CRC Press, Boca Raton, FL (1998)

Roy, A., Perfect, E., Dunne, W.M., Odling, N., Kim, J.-W.: Lacunarity analysis of fracture networks: evidence for scale-dependent clustering. J Struct Geol **32**(10), 1444–1449 (2010)

Stauffer, D., Aharony, A.: Introduction to Percolation Theory, 2nd edn. pp. 133 Taylor and Francis, London (1994)
Succi, S.: The Lattice Boltzmann Equation for Fluid Dynamics and Beyond. Oxford Science Publications, Oxford ISBN 0 19 850398 9 (2001)
Succi, S., Foti, E., Higuera, F.: Three-dimensional flows in complex geometries with the lattice Boltzmann method. Europhys. Lett. **10**(5), 433–438 (1989)
Sukop, M.C., Thorne, D.T.: Lattice Boltzmann Modeling—An Introduction for Geoscientists and Engineers. pp. 1–54. Springer, Berlin (2006)
Sukop, M.C., Dijk, G.J.van , Perfect, E., Loon, W.K.P.van : Percolation thresholds in 2-dimensional prefractal models of porous media. Transp. Porous Media **48**(2), 187–208 (2002)
Tarafdara, S., Franz, A., Schulzky, C., Hoffmann, K.H.: Modelling porous structures by repeated Sierpinski carpets. Physica A **292**, 1–8 (2001)
Turcotte, D.L.: Fractals and Chaos in Geology and Geophysics, 2nd edn. pp. 100–131. Cambridge University Press, New York (1997)
White, J.A., Borja, R.I., Fredrich, J.T.: Calculating the effective permeability of sandstone with multiscale lattice Boltzmann/finite element simulations. Acta Geotechnica **1**, 195–209 (2006)
Wolf-Gladrow, D.A.: Lattice Gas Cellular Automata and Lattice Boltzmann Models: An Introduction. Springer, Berlin ISBN 3-540-66973-6 (2000)
Xu, M., Eckstein, Y.: Statistical analysis of the relationships between dispersivity and other physical properties of porous media. Hydrogeol. J. **5**(4), 4–20 (1997)
Xu, P., Yu, B.: Developing a new form of permeability and Kozeny–Carman constant for homogeneous porous media by means of fractal geometry. Adv. Water Resour. **31**, 74–81 (2008)
Xu, Y.: Calculation of unsaturated hydraulic conductivity using a fractal model for the pore-size distribution. Comput. Geotech. **31**, 549–557 (2004)
Xu, Y.F., Dong, P.: Fractal approach to hydraulic properties in unsaturated porous media. Chaos Solitons & Fractals **19**, 327–337 (2004)
Yu, B.: Analysis of flow in fractal porous media. Appl. Mech. Rev. **61**(1–6), 0508011–05080119 (2008)
Yu, B., Liu, W.: Fractal analysis of permeabilities for porous media. Am. Inst. Chem. Eng. J. **50**(1), 46–57 (2004)